Final report

Contract Order Number: F61775-99-WE074

Surface evaluation of laser-irradiated coated / uncoated MIR optronic components

Wolfgang Riede
DLR Stuttgart
Institute of Technical Physics
Pfaffenwaldring 38 – 40
70 569 Stuttgart
Germany

Stuttgart, December 2000

REPORT DOCUMENTATION PAGE

Form Approved OMB No. 0704-0188

1. AGENCY USE ONLY (Leave blank)	2. REPORT DATE	3. REPORT TYPE AND DATES COVERED
	December, 2000	Final Report

4. TITLE AND SUBTITLE

Surface Evaluation Of Laser-Irradiated Coated/Uncoated Mid-IR Optronic Components

5. FUNDING NUMBERS

F61775-99-WE

6. AUTHOR(S)

Mr Wolfgang Riede

7. PERFORMING ORGANIZATION NAME(S) AND ADDRESS(ES)

DLR Stuttgart
Pfaffenwaldring 38-40,
Pffaffenwaldring 38-40
Stuttgart 70569
Germany

8. PERFORMING ORGANIZATION REPORT NUMBER

N/A

9. SPONSORING/MONITORING AGENCY NAME(S) AND ADDRESS(ES)

EOARD
PSC 802 BOX 14
FPO 09499-0200

10. SPONSORING/MONITORING AGENCY REPORT NUMBER

SPC 99-4074

11. SUPPLEMENTARY NOTES

Report is in Microsoft Word format on a CD.

12a. DISTRIBUTION/AVAILABILITY STATEMENT

Approved for public release; distribution is unlimited.

12b. DISTRIBUTION CODE

A

13. ABSTRACT (Maximum 200 words)

This report results from a contract tasking DLR Stuttgart as follows: The contractor will investigate the sensitivity of the scatter probe and photothermal deflection techniques for detecting the onset of laser-induced damage, and the applicability of these techniques for online, precursor laser-induced damage detection in mid-IR optical components irradiated with out-of-band radiation.

14. SUBJECT TERMS

EOARD, laser-induced damage

15. NUMBER OF PAGES

28

16. PRICE CODE

N/A

17. SECURITY CLASSIFICATION OF REPORT	18. SECURITY CLASSIFICATION OF THIS PAGE	19, SECURITY CLASSIFICATION OF ABSTRACT	20. LIMITATION OF ABSTRACT
UNCLASSIFIED	UNCLASSIFIED	UNCLASSIFIED	UL

Contents

1. Introduction

The laser damage facility at DLR, Institute of Technical Physics, is primarily based on the application of the small-spot technique for 1/1 or S/1 investigations according to the IS0 standards 11254-1.2 and 11254-2, respectively [ISO, Riede]. These standards provide a procedure for determining the laser-induced damage threshold of optical surfaces (coated or uncoated), where each site is exposed with one or more laser shots. As laser damage is defined any permanent radiation induced change in the surface of the sample that can be inspected by Nomarski DIC with a magnification of 100X to 150X. The damage threshold is defined to be that energy density or power density (in case of cw radiation) of laser radiation impinging on an optical surface above which the probability of damage is finite.

The primary task of the laser damage facility at DLR is to measure out-of-band LIDTs of optical components used in the infrared spectral range as these data usually cannot be found in the literature. Several pulsed laser sources within the spectral range 1 – 10 μm are available. The laser source used for experiments reported here is a pulsed, 10 Hz repetition frequency Nd:YAG laser providing a Gaussian intensity distribution on the sample. Under test were coated and uncoated samples consisting of different substrates. These samples were exposed to the 1.06 μm radiation, and single (1/1) and multiple pulse (S/1) damage thresholds were measured. A detailed description of the laser damage facility at DLR and out-of-band damage measurements of defense related materials is given in Chap. 2 and 3 of this report.

As the optical components used in laser optics are often very expensive (e.g. nonlinear crystals, laser crystals) irradiation of these components should be stopped prior to massive damage has occurred on the surface or in the bulk.

If a practical, inexpensive method for detection of low-level damage sites during operation of laser system would be available laser downtime could be reduced. Additionally, massive bulk damage could be prevented and simple repolishing of the damage faced would be sufficient. Photothermal deflection was considered to be a method that can be used to monitor low-level and even pre-damage effects as in several reports in the literature damage precursors are being mentioned [e.g. Welsch] but there is no such application yet.. Hence, the potential of the PTD technique with respect to the mentioned methods will be described in this report and a comparison between PTD and scatter probe techniques (SPT) was performed with respect to the sensitivity of damage assessment (Chap. 4,5).

2. Detailed description of damage apparatus at DLR laser damage lab

The laser source used for the experiments of this report is a commercial Nd:YAG laser (BMi, France) producing pulses of 13 ns duration in TEM_{OO} mode at 10 Hz repetition rate. The laser damage system (c.f. Fig. 2.1) at DLR is completely automated. The data acquisition and instrument control is accomplished via IEEE interface. The laser pulse energy density on the sample is varied by a rotatable, computer-controlled $\lambda/2$ plate positioned between two polarisers. This allows a variation of the laser pulse energy on the sample from 100 µJ up to 70 mJ. Reflected signals from a wedge are used to measure the pulse energy of each pulse. Two identical lenses L1, L2 of focal length f = 1 m focus the beam on the sample and the beam profile analysis unit, respectively. Data from beam profile analysis and pulse energy monitoring are transferred to the PC. The sample is fixed to and positioned with a motorized, computer-controlled x-y-z translation stage and is scanned along a rectangular grid with a grid dimension of 1 mm. The shutter unit reduces the repetition rate of the irradiation of the sample down to 0.1 Hz when operating in the 1/1 mode. In case of the S/1 mode, the shutter is necessary for an extended exposure of the sample at 10 Hz pulse repetition rate. The beam profile on the sample was measured with a Pt-Ir pinhole of 20 µm diameter (Fig. 2.2). It is of Gaussian shape with $1/e^2$ diameter of 460 µm. Nomarski DIC and scanning force microscopy allow for the final decision on laser damage and for investigation of the damage morphology.

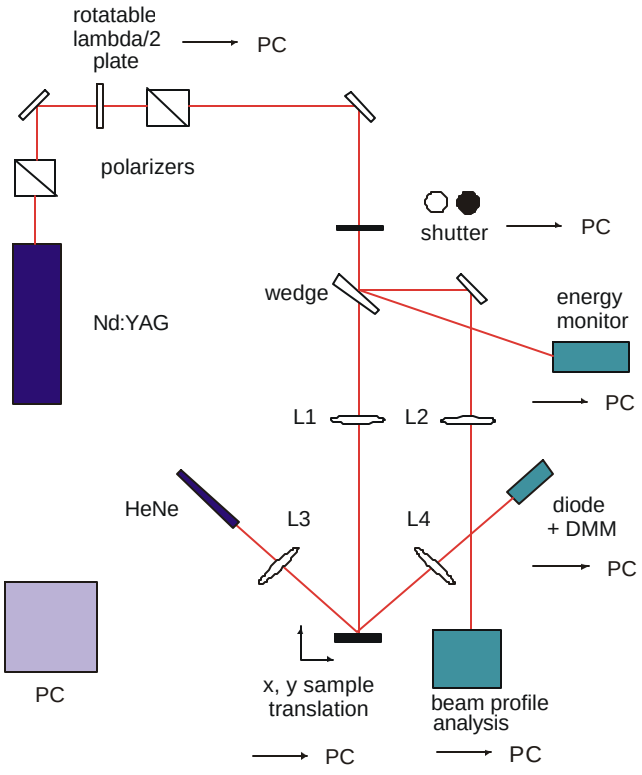

Fig. 2.1 Damage apparatus.

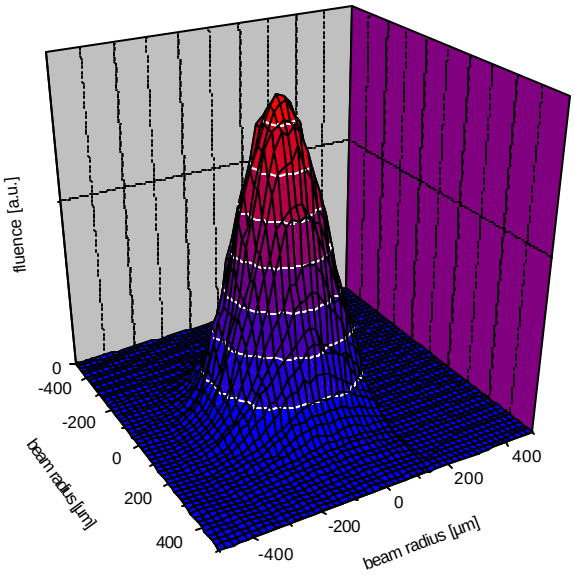

Fig. 2.2 Beam profile

For online damage assessment, the scatter probe technique (SPT) is utilized [Franck]. Fig. 2.3 depicts the details. The sample is illuminated with light provided by a stabilized HeNe laser. The HeNe laser beam is focused with a lens (f = 200 mm) and reflected off the two sample surfaces (in case of transparent samples). The HeNe laser radiation has its waist on the first surface of another lens (f = 100 mm) which collects the scattered light and blocks the specularly reflected light by an

opaque spot. A battery powered photodiode detector connected to a digital multimeter (DMM) is used to monitor the scattered light. A HeNe transmission filter and a Nd:YAG blocking filter in front of the detector are used to increase the signal to noise ratio. The light amplitude measured with the photodiode is increased when a surface modification due to laser interaction with the sample occurs. Depending on the sample surface (cleanliness, polishing quality) a certain increment will always be significant of a damaged site. The scatter probe technique can be implemented into an automated system (in-situ, non-invasive) and can provide an objective criterion for the occurrence of damage either on front or back surface. Another advantage is that it works independently of the kind of laser-induced surface modification like melting or coating ablation.

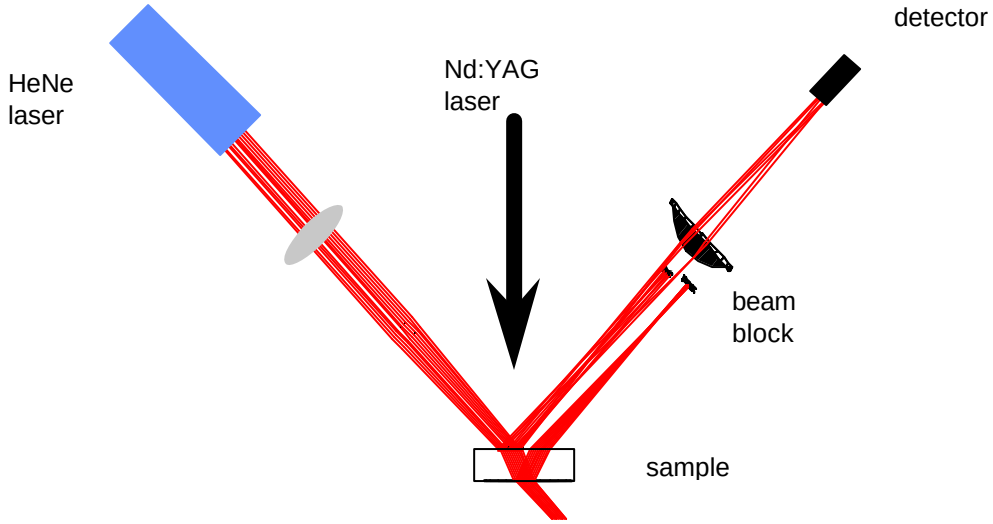

Fig. 2.3 Scatter probe setup.

The SPT is used at DLR laser damage lab for several years in automated damage assessment, and its sensitivity is comparable to Nomarski microscopy (which has to be used according to ISO 11 254 1.2/2.0). Problems arise in sensitivity when the sample surface is highly scattering and when it is not perfectly clean. Then, the cleaning effect by laser irradiation, i.e. a reduction in scattered amplitude, may dominate the increase in scatter due to damage.

3. Out-of-band damage measurements of defense-related materials

The specifications of the samples that were damage tested are summarized in the following

Tab. 3.1.

Substrate	*Coating*	*Diameter [mm]*	*Thickness [mm]*	*Surface Quality (s/d)*	*Absorption length $1/\rho_T$ @ 1.064 µm [mm]*
ZnSe	_	50.8	5	40/20	2000
ZnSe	AR/AR @ 10.6 µm	50.8	5	40/20	
Ge	_	30	3	40/20	0.0007
Ge	AR/AR @ 10.6 µm	30	3	40/20	_
Si	_	50.8	3	-	1.27
Sapphire	AR @ 3 – 5 µm	38.1	2.5	60/40	

Tab. 3.1 Specifications of investigated samples.

3.1 ZnSe samples

The results on the LIDT measurements with coated and uncoated ZnSe samples are shown in Fig. 3.1a - c and 3.2a - c. In the inset, the sample type and its corresponding laser damage threshold (LIDT), the overall number of shots, and the irradiation mode are specified. Single and multiple pulse data were taken from one sample of each type. Each damage threshold is derived by extrapolating a straight line through a few data points above zero probability and evaluating its intersection point with the abscissa of the probability curve (c.f. Chap. 8.1). In case of the ZnSe substrates a distinct drop in threshold is observed when the number of shots per site is increased. The measured values are 4.2, 3.8 and 1.8 J/cm² for 1/1, 10/1, and 100/1 irradiation mode. This drop can certainly not be explained with a stochastical effect (i.e. due to an increased number of pulses). More likely, an accumulation effect must be the cause. The corresponding LIDT measurements for the AR coated samples are depicted in Fig. 3.2a - c. A very small decrease in threshold (2.8 - 2.4 J/cm²) with increasing number of laser shots can be concluded from these figures. Therefore, accumulation effects played a minor role with the AR coated samples.

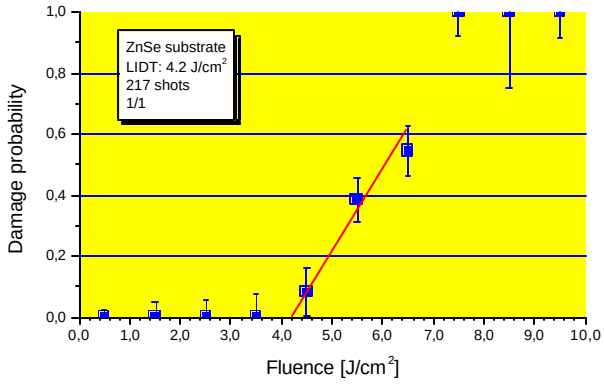

Fig. 3.1a ZnSe substrate, 1/1 mode

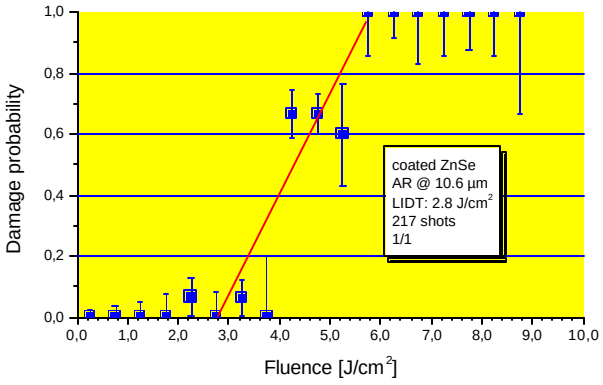

Fig. 3.2a ZnSe AR @ 10.6 µm, 1/1 mode

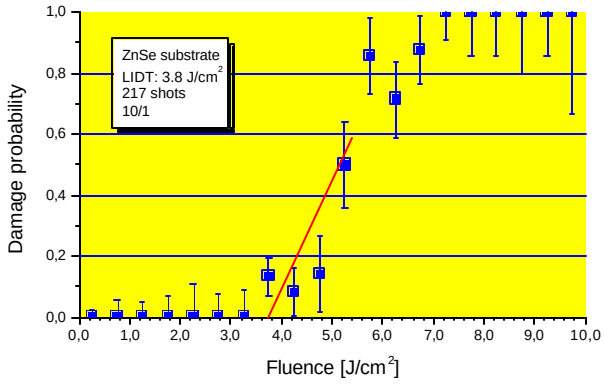

Fig. 3.1b ZnSe substrate, 10/1 mode

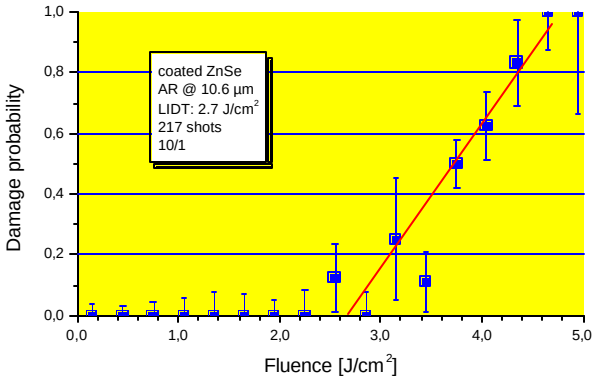

Fig. 3.2b ZnSe AR @ 10.6 µm, 10/1 mode

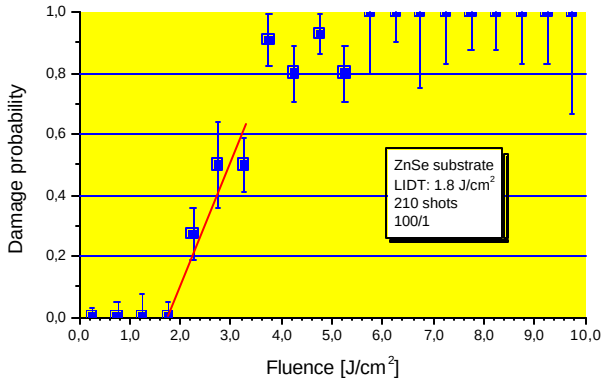

Fig. 3.1c ZnSe substrate, 100/1 mode

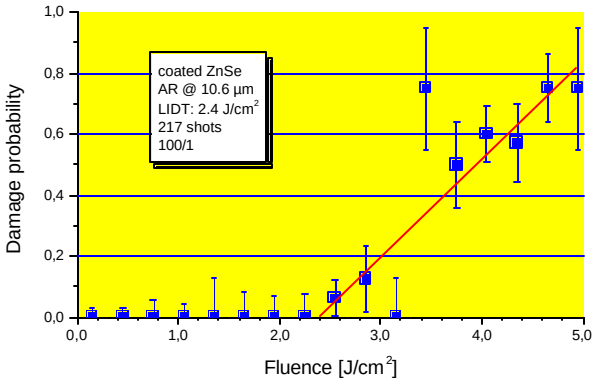

Fig. 3.2c ZnSe AR @ 10.6 µm, 100/1 mode

SPT was applied to keep track of the damage development during multipulse (S/1) irradiation.

The repetition rate was set to 10 Hz. Damage manifested itself in the scattered light for fluences between 3 - 4 J/cm² as a stepwise increase in the amplitude (c.f. Fig. 3.3). This is attributed to an increase in the number of scatter centers in the front surface.

At higher fluences, damage became catastrophic, leading to very high amount of scatter (Fig. 3.4). The damage morphology was melt craters on the surface, especially with severe damage on the back surface and even bulk damage.

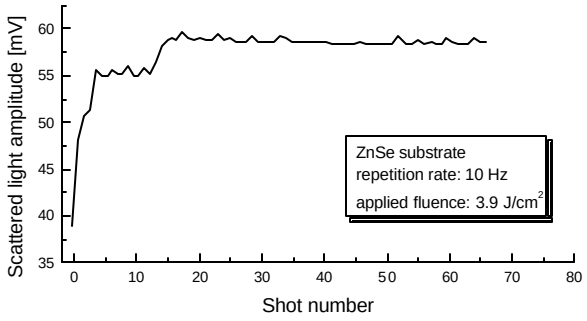

Fig. 3.3 Temporal development of scatter

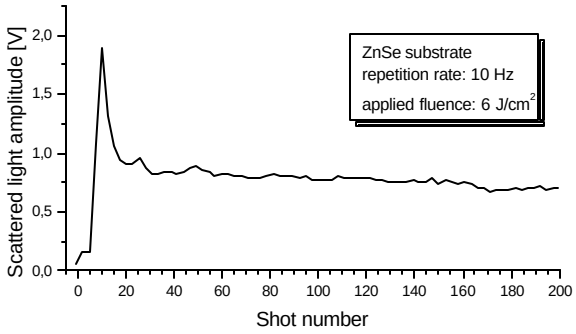

Fig. 3.4 Temporal development of scatter (F = 3.9 J/cm²) (F = 6 J/cm²)

In Nomarski microscopy the front surface damage appeared as distributed damage. A closer investigation of these sites revealed the damage morphology as pits, which were for both ZnSe substrates and AR coated windows approx. 0.5 µm deep and a few microns wide (Fig. 3.5).

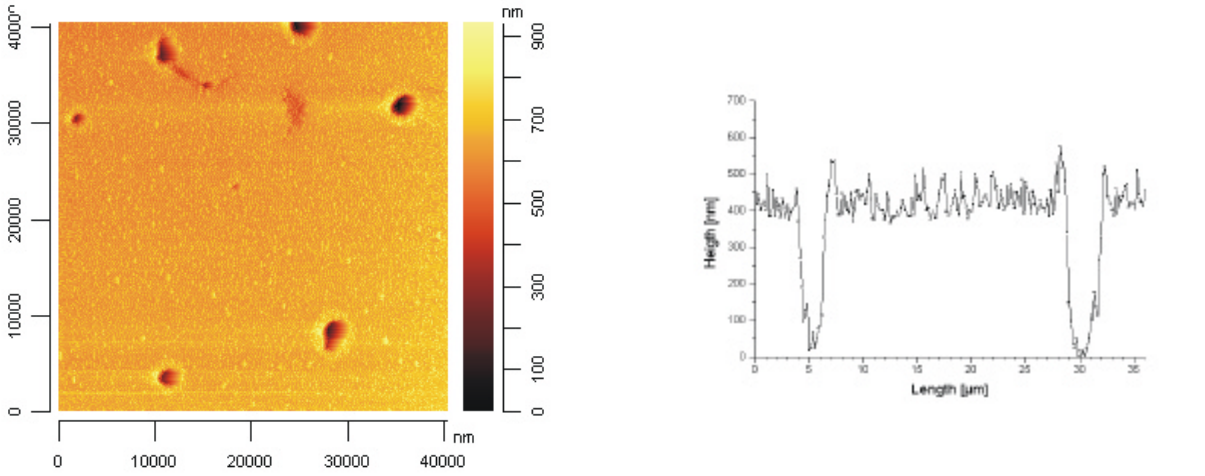

Fig. 3.5 Topography of front surface damage on ZnSe substrate.

3.2 Ge samples

The penetration depth of Nd:YAG laser radiation in Ge is very small (0.7 µm, Tab. 3.1). Therefore, a low damage threshold can be expected.

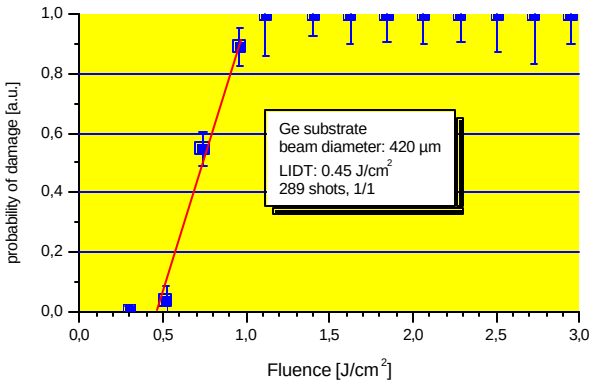

Fig. 3.6 Ge substrate, 1/1 mode.

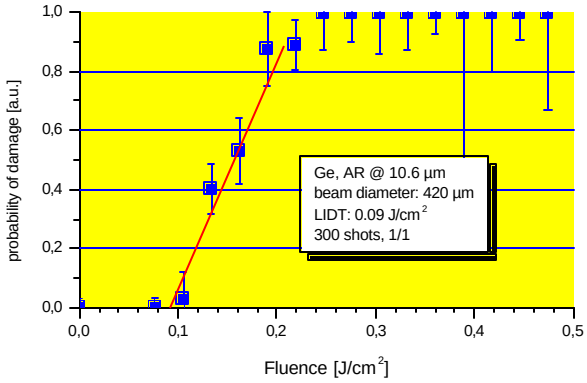

Fig. 3.7 Ge AR @ 10.6 µm, 1/1 mode.

A threshold of 0.45 J/cm² was measured for bare Ge substrates (Fig. 3.6). The coated substrates had an even lower threshold of 0.09 J/cm² (factor 5) than the uncoated samples. This is shown in Fig. 3.7. The probable cause of the difference might be due to the coating lift-off as a consequence of substrate absorption and bulging. Therefore, coating delamination was found in case of coated Ge substrates (Fig. 3.8, left) and melt craters in case of the uncoated Ge substrates (Fig. 3.8, right).

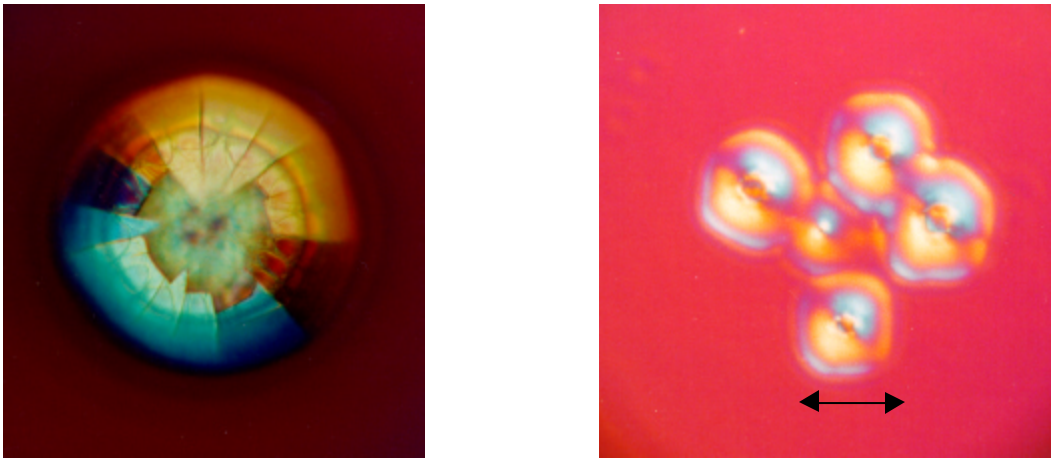

Fig. 3.8 Nomarski micrograph of delaminated coating on Ge (left, diameter 89 µm) and melt craters on Si (right, diameter 25 µm, indicated by the arrow).

3.3 Si samples

Si and Ge show a similar damage morphology. In the first stage of low level damage, an increasing surface roughness and apparent surface melting can be observed. In case of medium level damage, a small circular structure (melt crater) can be found on the surface (Fig. 3.8, right). An increase in scatter amplitude can be attributed to crater rims.

The damage threshold for Si was found to be higher than for Ge. The explanation lies certainly in the lower absorption (c.f. Tab. 1) of Si at 1.06 µm. For Si substrates, LIDTs of 1.9, 1.65 and 1.55 J/cm² were measured for 1/1, 10/1 and 100/1 irradiation mode (Fig. 3.9).

In Tab. 3.2, the results of the LIDT measurements on the set of samples are summarized.

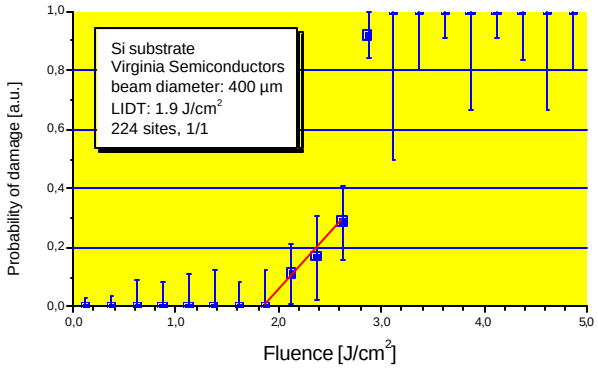

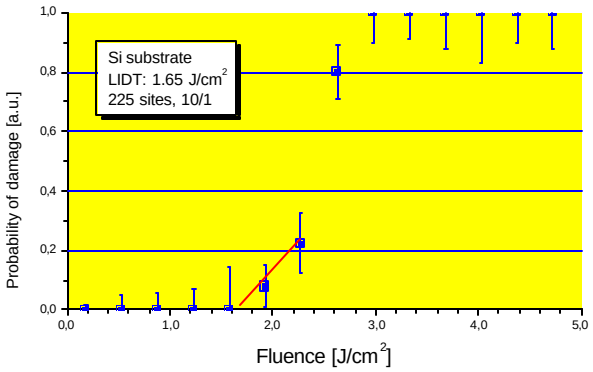

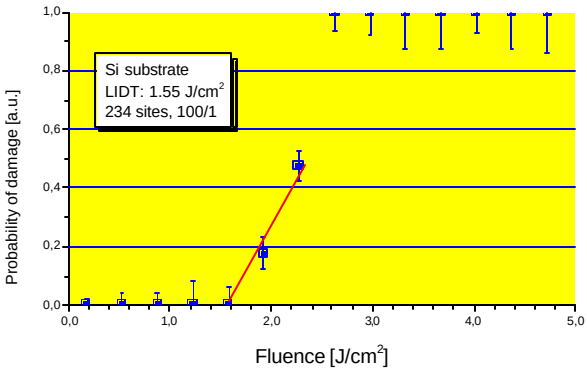

Substrate	*1/1*	*10/1*	*100/1*
ZnSe	4.2	3.8	1.8
ZnSe, AR/AR	2.8	2.7	2.4
Ge	0.45	–	–
Ge, AR/AR	0.09	–	–
Si	1.9	1.65	1.55
Sapphire	~ 12.5*		

Tab. 2 Measured damage thresholds in [J/cm²] for single and multipulse irradiation (at 10 Hz). (*: data based on PAD).

Fig. 3.9 LIDT measurements of Si substrate.

4. Comparison of techniques for damage monitoring

Damage precursors are not a general phenomenon but depend strongly on the kind of material examined. In literature, several precursor techniques can be found.

Among them are effects which do accompany dielectric breakdown and subsequent damage [Domann_a,b,c]. The conductivity increases (e.g. in alkali-halide crystals) and charged and neutral particles will be emitted upon irradiation at subthreshold levels (CdS, Si). With fused silica samples with ThF_4 coating no subthreshold precursors were found [Becker]. The measurement of the existence of charged particles is very cumbersome and affords vacuum mass spectrometry equipment. Consequently, there is no way to implement such a system as a non-expensive add-on to an existing laser application. Additionally, no correlation between charge emission and subsequent damage was reported in the papers listed [Domann_a,b,c].

Measurements on the photo-emission of charged particles from diamond-like carbon films on silicon substrates used for determining the ablation threshold are reported in [Vouagner]. Experiments are performed in a UHV chamber under application of high voltage between sample (anode) and a cathode.

A more practical measurement scheme is based upon using high resolution Schlieren imaging to monitor the deflection of a pulsed probe beam right after applying a subthreshold pulse from the test laser [Clark]. Good spatial correlation for forecasting damage sites is claimed. Still, this method is unsuitable for the observation of optics exposed to laser radiation.

In [Rosencwaig_a,b,c], a method is developed of observing the occurrence of laser damage by transducer detection of damage-generated acoustic waves inside the sample. Absorbed laser light is converted into heat and generates an acoustic shock wave that can be measured by a transducer. The disadvantage is that this method affords a bonding contact with the sample and that the correlation to damage is obvious only by an *increase* in signal as a photoacoustic signal inside the sample is *always* produced whenever laser light is absorbed by dielectric films.

The scatter probe technique, SPT [Franck], is commonly referred to as the most sensitive method [Petzhold] for detection of surface morphology changes but it can only report on damage that has already occurred on the sample surface. On the other hand, SPT was shown to predict damage initiation sites on well-polished samples [Porteus]. First, a scatter mapping with a probe laser beam has to be performed. Subsequent irradiation showed good correlation of damaged sites with highly scattering sites. Still, it cannot be used for online damage prediction. Due to its high sensitivity which is confirmed by practical experiences from damage measurements at DLR damage lab it can perfectly be used together with Nomarski microscopy inspection as the definition of onset of damage.

The photoacoustic / photothermal deflection (PAD/PTD) is compared to most of the above-mentioned techniques, with the exception of the SPT, a simple, online and non-contact method. Its principle will be explained in the following Chap. 5. Due to [Petzhold] it allows for a reliable in situ determination of damage thresholds. Additionally, in [Welsch] a distinct transition of the acoustic signal is reported when exceeding the damage threshold.

5. Application of SPT and PAD/PTD

5.1 Principle of PAD/PTD

The photothermal or photoacoustic deflection (PTD/PAD) which is also called mirage effect is based on the deflection of a cw probe laser beam being adjusted parallel to the surface of a sample that is irradiated with a pulsed laser and prone to damage. The interaction of the laser pulse with the sample (absorption, plasma production, ablation) generates acoustic and thermal waves that start to propagate from the sample surface into free space. When these waves intersect the cw laser beam, an angular deflection will occur that can be monitored. This monitoring is usually done via quadrant detectors or with knife-edge techniques [Petzoldt]. Here, a newly developed sensitive method of angular deflection detection will be presented. It is based on the total internal reflection (TIR) using a prism (therefore called TIR based PAD/PTD). The principle of TIR based PAD/PTD can be inferred from Fig. 5.1 and from the photograph in Fig. 5.2.

Fig. 5.1 Setup for photothermal deflection measurement. The HeNe laser is probing the back surface of the sample.

A stabilized HeNe laser (Spectra-Physics, 1.4 mW, intensity stability ± 0.1%) is passing at approx. 1 mm distance from the

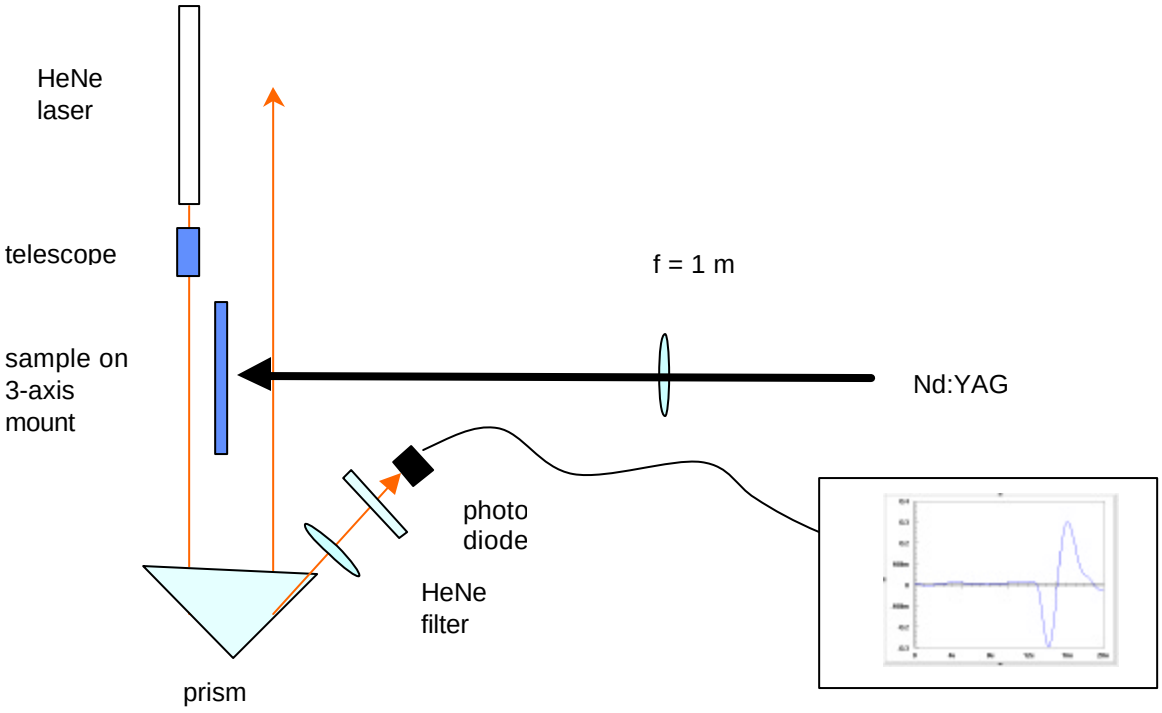

surface that is to be investigated. Due to thermal and acoustic waves that diffuse and propagate through the HeNe laser beam, an angular deflection will occur. If the prism is adjusted such that one of its minor faces is near the total internal reflection angle, then the transmission through this plane will be a function of the angle, and can be monitored with a photodiode, as shown in Fig. 13. The photodiode is equipped with a HeNe transmission filter and a Nd:YAG blocking filter. A typical signal measured is shown in the inset (DSO). The peak to valley amplitude is used as the strength of this signal.

Fig. 5.2 Photograph of scatter probe and PAD/PTD setup. The probe beam is entering the scene from the lower right and is propagated along the back side as well as along the front side of the sample.

A detailed view of the rays reflected and transmitted at one of the minor faces of the right angle prism is depicted in Fig. 5.3., showing the angles as well.

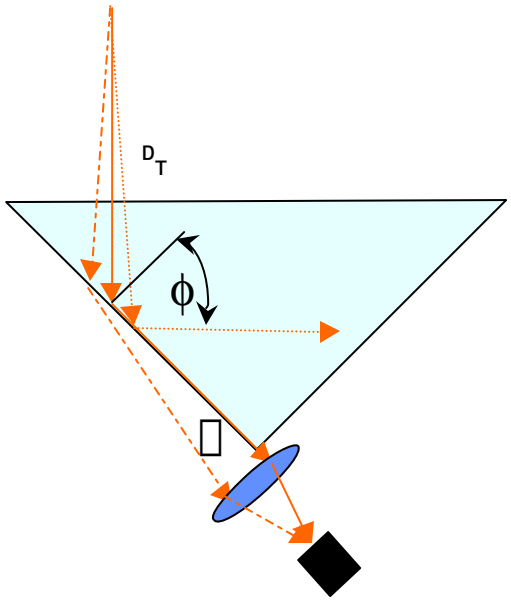

Fig. 5.3 Detailed view of ray propagation.

The angle of total internal reflection $^{s}_{sc}$ is given by:

$^{s}_{sc}$ = arcsin(1/n) = 43.4 °, n_{quartz}(= 0.632 µm) = 1.4572.

Using the common Fresnel relations for the involved surfaces, (hypotenuse face = entrance face, minor face = exit face) the transmission through the minor exit face as a function of the deflection angle $^{D}_{T}$ can be calculated. This is shown in Fig. 5.4 for s-polarized light. The calculation is valid for parallel rays of light. To minimize the effect of laser beam divergence (which will reduce the slope of the transmission curve in Fig. 5.4) the HeNe beam waist was positioned - using a HeNe laser

telescope - near the exit face of the prism. In the experiments the prism was tilted more than the exact TIR angle to some work point on the transmission curve (blue circle in Fig. 5.4). Typically, the deflection angles are smaller than 1 mrad.

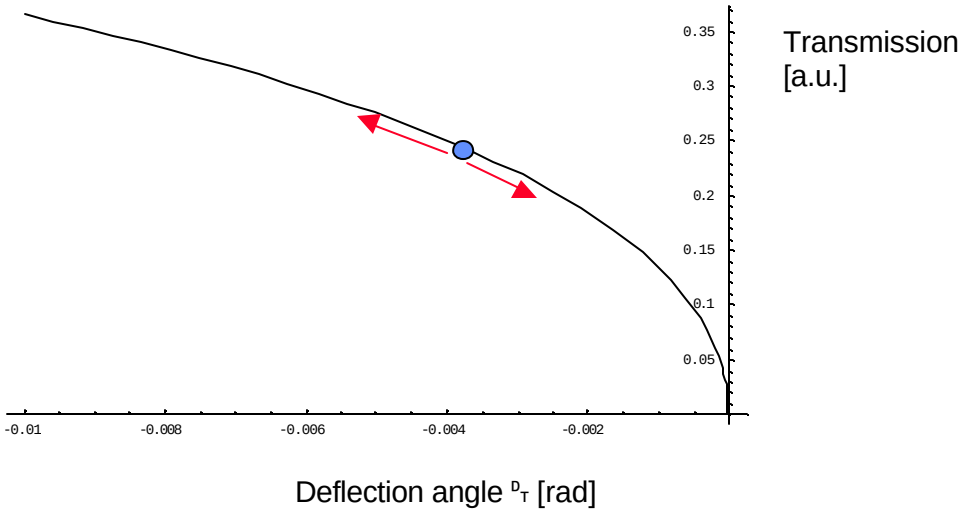

Fig. 5.4 Prism transmission as a function of the deflection angle for s-polarized light.

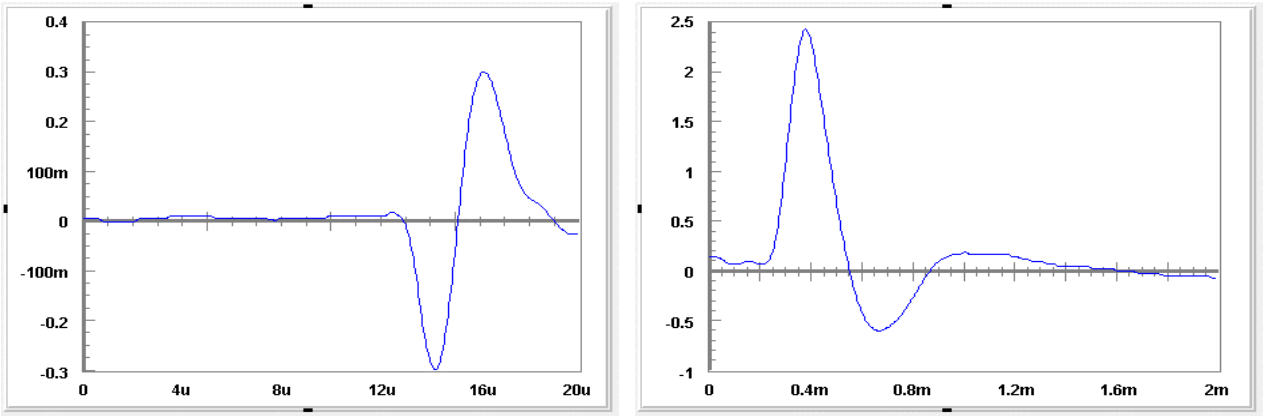

Fig. 5.5 Typical oscilloscope traces of photoacoustic (left) and photothermal signals (right). (Time scale in µs (left) and ms (right)). Peak-to-valley excursion was used as a measure for the strength of signals. (Shock wave duration: 5 µs, thermal wave duration: 600 µs)

Typical signals are shown in Fig. 5.5, with the photoacoustic signal depicted on the left and the photothermal signal an the right. The signals have a different shape and different propagation velocities. The propagation of the thermal signal is based on diffusion whereas the photoacoustic signal propagates initially as a (hypersonic) shock wave where compression followed by dilution. Anyhow, the spatial extension of the acoustic shock front and thermal signature are typically 2 mm, i.e. are identical. The source of the thermal signal is the (damaged) surface area which is heated by radiation absorption, whereas ablation and plasma is usually accompanied by shock waves (for velocity measurements, c.f. Figs. 5.6/5.7).

The deflection angle ϑ_T of the probe beam direction is given by

$$a \propto \frac{\partial n}{\partial T}\frac{\partial T}{\partial z}dz + \frac{\partial n}{\partial p}\frac{\partial p}{\partial z}dz$$

where the terms are responsible for the thermal (left) and the shock-wave branch (right), respectively, which are operating in distinct time regimes.

8.2 Measurements with Si

PTD measurements were done with Si wafers and sapphire windows as the samples.

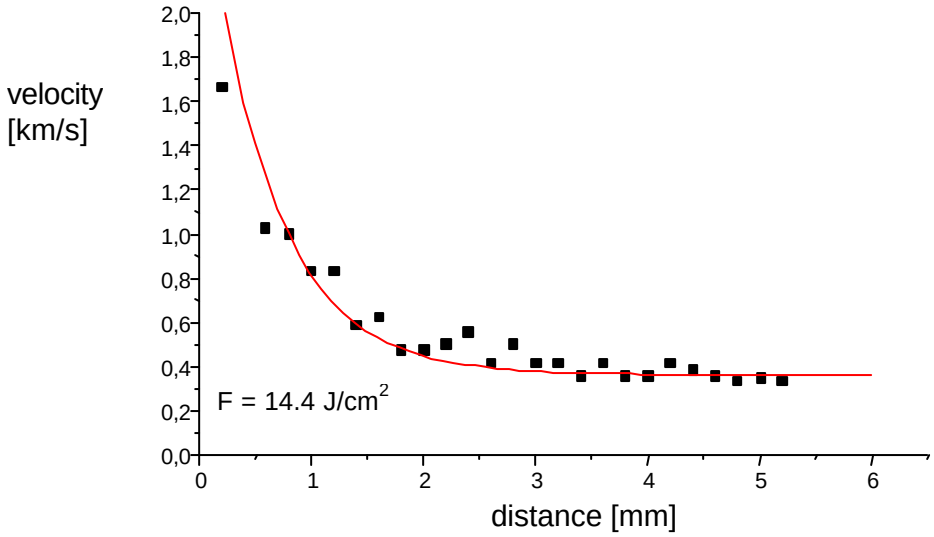

Fig. 5.6 Acoustic wave velocity vs. distance above Si wafer.

The shock wave velocity above Si (Fig. 5.6) initially exceeds the sonic speed (340 m/s) by far and reaches acoustic velocity after several mm of propagation. The thermal wave on the other hand propagates at a speed of several m/s only (Fig. 5.7).

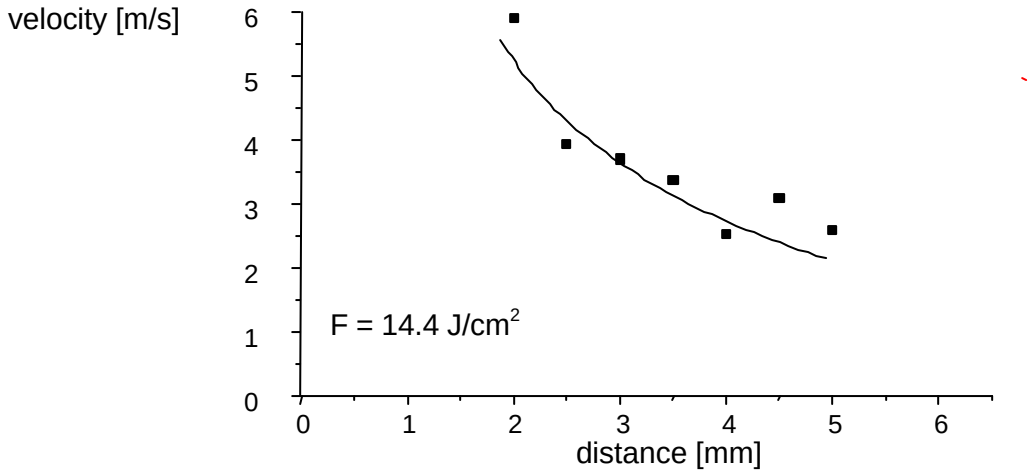

Fig. 5.7 Thermal wave velocity vs. distance above Si wafer.

The amplitudes of thermal and acoustic waves as a function of the applied fluence were considered to be an important parameter in order to determine the threshold of the involved effects. As can be seen from Fig. 5.8., the thermal signal disappears at about 3 J/cm² whereas the acoustic signal can still be detected at lower fluences down to 2 J/cm². When comparing these data with the 1/1 damage threshold measurement of Si (Fig. 3.9), an acoustic amplitude still can be observed at fluences near the LIDT of Si. As this may be influenced by sample to sample variations (the LIDT measurements from Chap. 3 and the PTD measurements of this Chap. were done with different samples from the same vendor), the irradiated sites were viewed at the microscope. When the acoustic amplitude was smaller than 20 mV and well above the detection limit of 10 mV, no damage surface structure could be observed. When the thermal wave was observed via PTD at fluences greater than 3 J/cm² severe damage could be seen with phase contrast techniques using a microscope.

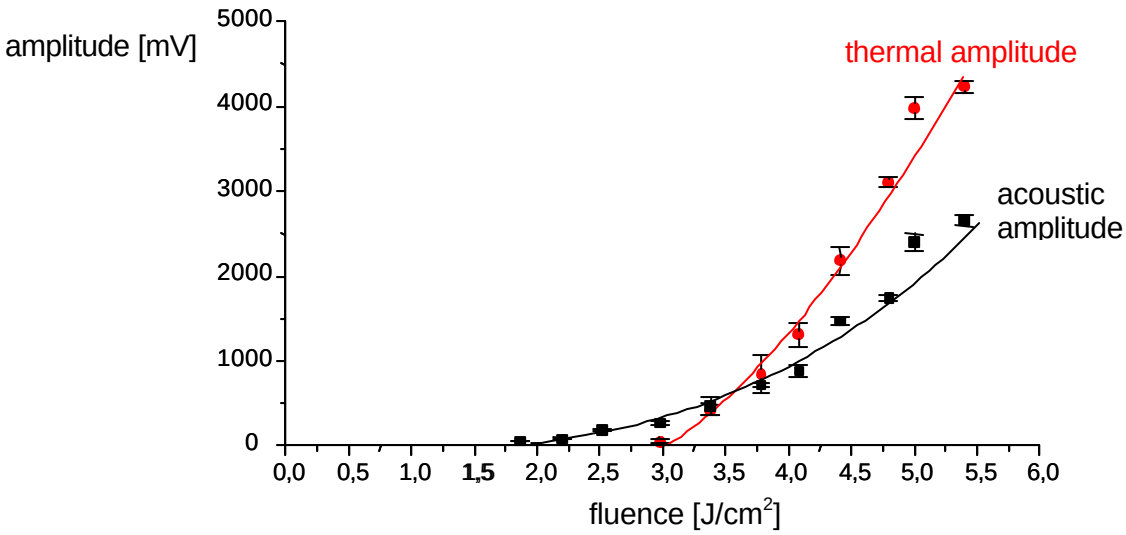

Fig. 5.8 Threshold behavior of thermal and acoustic wave above Si. The amplitude is the peak to valley voltage difference of the corresponding oscilloscope traces.

Consequently, the TIR-based PAD/PTD can be considered to be a sensitive method of monitoring the damage behavior of Si under Nd:YAG irradiation.

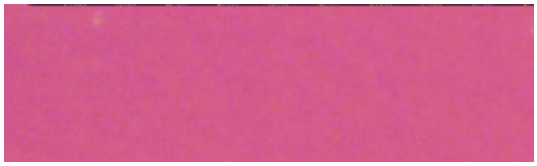

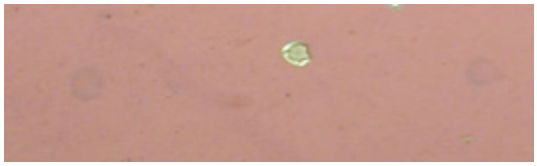

Fig 5.9 Left: Damage morphology of low level damage on Si (F = 5 J/cm²). The melted area on the right has a diameter of only 6 µm. Right: Damage morphology of low level damage on the front surface of sapphire (F = 14.9 J/cm²). The coating is delaminated at several sites.

An example of a damaged site of Si is shown in Fig. 5.9, left, where a fluence of = 5 J/cm² was applied and the acoustic and thermal amplitudes were 9 mV and 0 mV, respectively.

5.3 Measurements with sapphire

The sapphire samples show a small but distinct absorption near 1.06 µm of nearly 2% (Fig. 5.10). The spectral absorption (A) was attained from reflectance (R) and transmittance (T) FT-IR spectrometer scans using: 1 = R + T + A.

Fig. 5.10 Spectral absorption of coated sapphire samples (AR coating for 3 – 5 µm) near 1.06 µm wavelength.

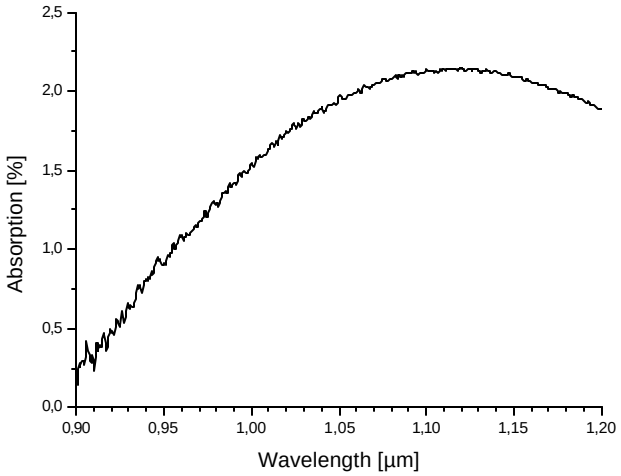

This absorption must be attributed to absorption in the coating and not in the bulk. As in the case of Si samples, a thermal wave and an acoustic wave was observed, where again the acoustic wave was observable down to smaller fluence values than the thermal wave. The sapphire samples were used for a comparison between the SPT and TIR-based PTD, the result is depicted in Fig. 5.11. Low level damage of sapphire front surface is shown in Fig. 5.9, right.

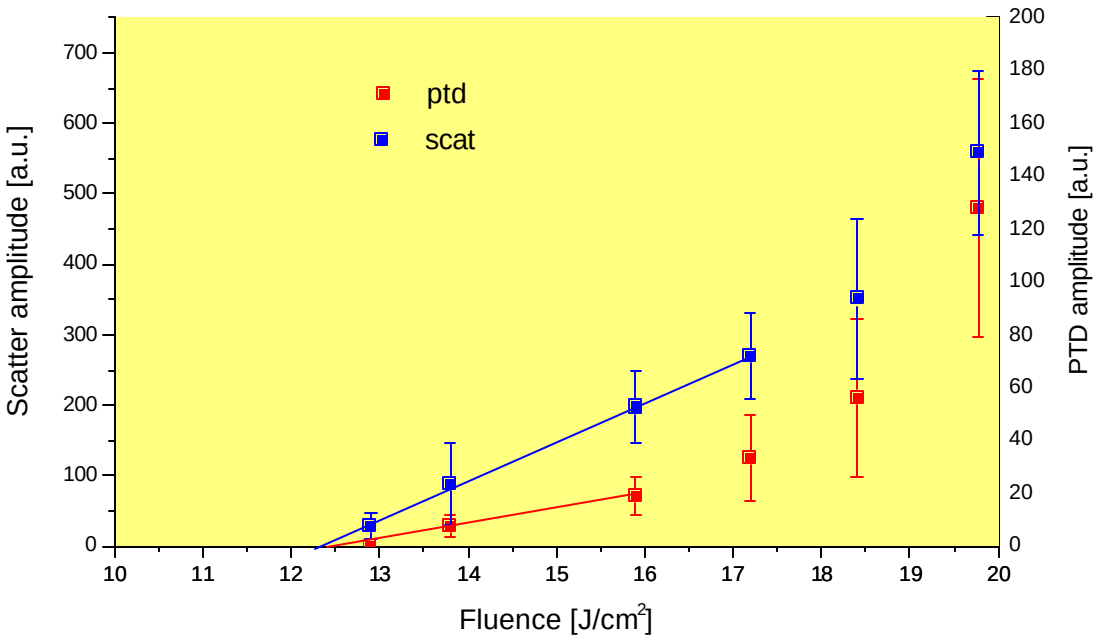

Fig. 5.11 Comparison of sensitivity of SPT (blue trace, left abscissa) and TIR-PTD (red trace, right abscissa) with sapphire samples. At each fluence the value of the average of 10 measurements was taken. (PAD signal : 100 mV ≅ 200 µrad, sensitivity ≈ µrad)

Within the error margins, the SPT seems to be more sensitive than the TIR-based PAD, especially near threshold. Anyhow, a linear fit of the last 3 – 4 data points yields the same threshold of approx. 12.5 J/cm².

TIR-based PTD can be used to monitor the different faces of a sample when the probing laser beam is propagated at different distances from the corresponding faces. In Fig. 5.12 the photoacoustic signal due to consecutive shots at the same site on a sapphire sample is shown. As the sample is practically transparent, front and back surface damage will occur. Typically, the first shot produced front surface damage which stagnated then whereas consecutive shots lead to increasing damage on the back surface. By inspection, the damage was found to propagate into the bulk.

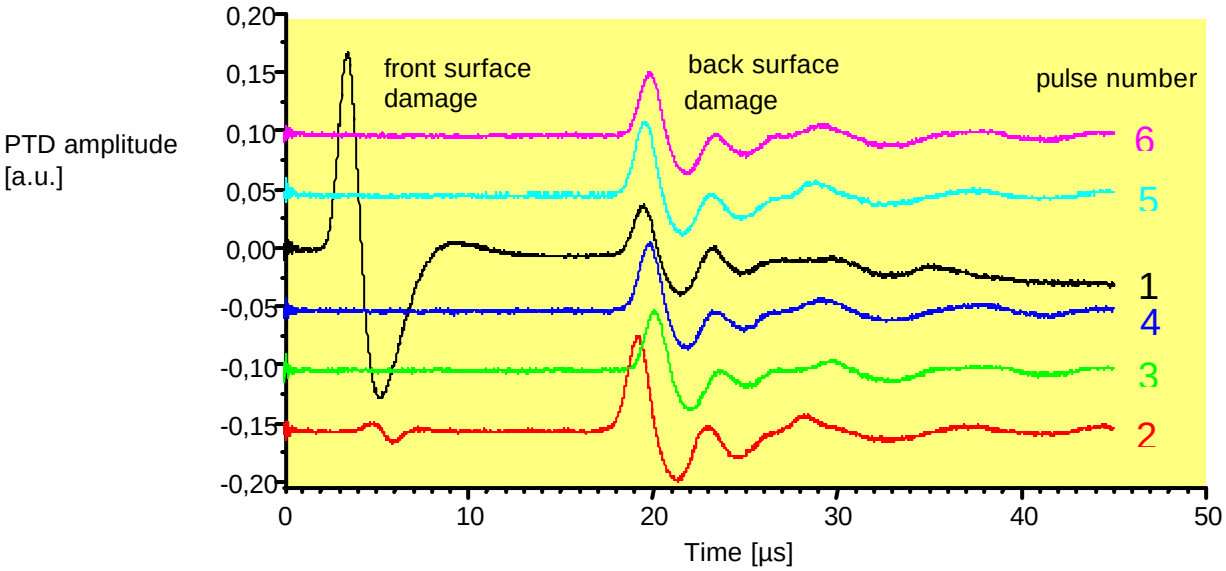

Fig. 5.12 Oscilloscope traces of the PTD amplitude of consecutive shots at the same site on a sapphire sample with F = 26 J/cm². Front and back surface damage can be discriminated as they appear at different times after the laser pulse (trigger) at t = 0 µs.

5.4 Measurements with BK7

BK7 glass has a rather high damage threshold as its intrinsic absorption is usually very low, on the order of 10 ppm [Willamowski]. Threshold assessment of BK7 is shown in Fig. 5.13, and a value of 65 J/cm² can be inferred for 1/1 irradiation of the back surface at 1.06 µm wavelength.

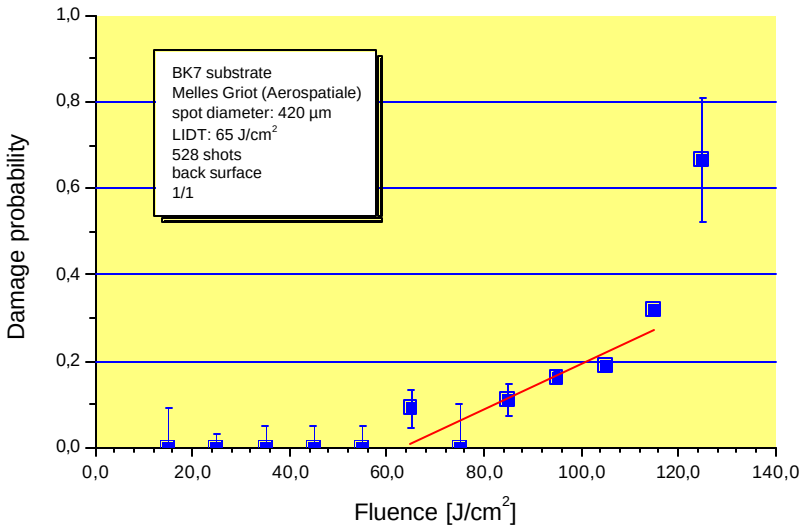

Fig. 5.13 Measurement of the damage threshold of BK7 substrate (back surface)

The damage morphology between front and back surface is pretty different (Fig. 5.14). On the front surface, a plasma scald is surrounding the absorbing site, from which the plasma has emanated. The plasma is shielding the surface, just in contrary to the rear surface, where the plasma is ignited in the bulk near the surface. Consequently, the damaging effect is greater.

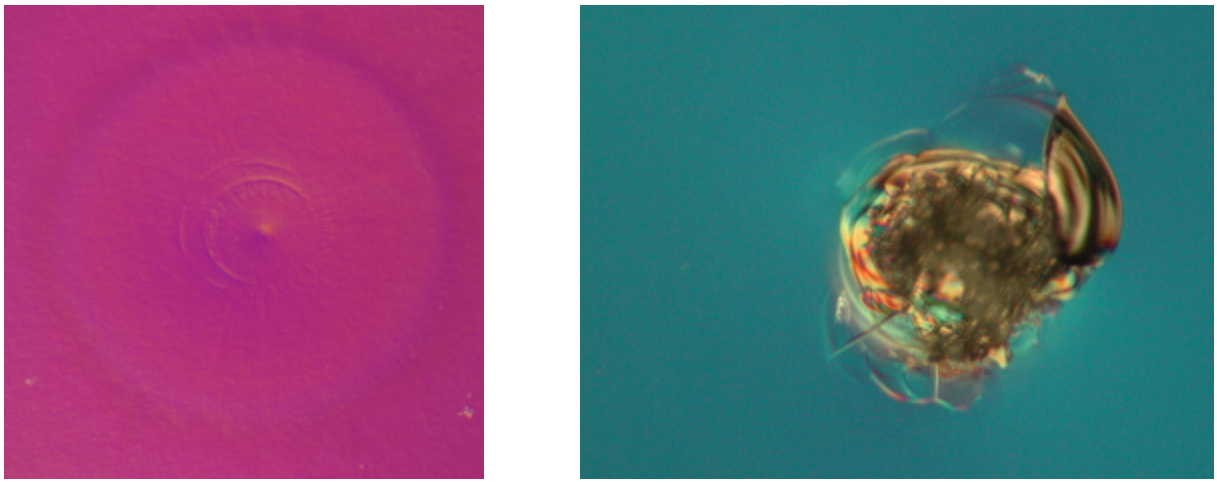

Fig. 5.14 Typical damage morphology of BK7 front surface (left) and back surface (right) damage.

The setup as shown in Fig. 5.1 / 5.2 was extended by a third signal channel, the plasma flash, which was imaged by some lens on another photodiode. By applying the same statistical methods to acoustic, scatter and plasma measurements (Chap. 8.1), a probability vs. fluence curve could be plotted (Fig. 5.15). At first glance very surprisingly, a perfect match of probability was found especially between scatter and acoustic data. The extrapolated thresholds differ only slightly (scatter: 21.6, plasma: 20.56, acoustic wave: 21.56)

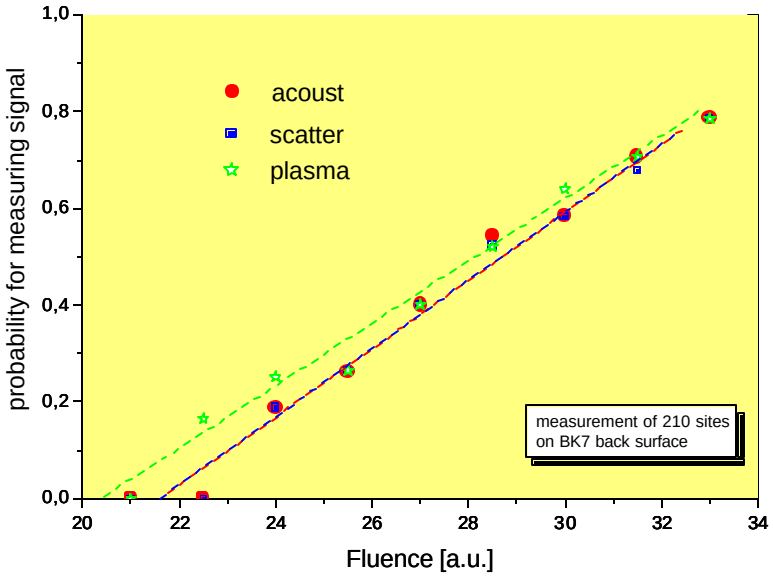

Fig. 5.15 Comparison of threshold behavior of different physical effects occurring near the back surface of BK7 after the irradiation of BK7 back surface. The fluence is plotted here in arb. units (for LIDT value, c.f. Fig. 5.13)

The explanation is very evident as this strong statistical correlation points to a strong correlation of the underlying physical processes: The only possibility of damaging the rear surface of the sample under the given experimental circumstances (wavelength, laser pulse duration, sample etc.) is via plasma ignition. Plasma ignition is always correlated to the generation of an acoustic wave and plasma (if detected) will always lead to damage measurable by increased scatter.

6. Summary and outlook

In this report results of laser damage threshold measurements at typical MIR optical components (Ge, Si, ZnSe, sapphire) are summarized. These components were damage tested under out-of-band, pulsed irradiation at 1.06 µm.

A new technique of monitoring laser-induced shock waves and thermal waves above the sample surface called TIR-based PAD/PTD was developed and tested and found to be a sensitive and practical tool.

With PAD detection selective monitoring of several sample surfaces of optical components can be realized, irrespective of their thickness. Therefore, PAD might be used as a tool for online monitoring of expensive laser crystals or nonlinear-optical systems to prevent irreversible damage. A corresponding damage monitor has been proposed.

TIR-based PAD/PTD technique has been applied to materials having a very low LIDT due to very strong absorption and BK7, where the damage mechanism was identified being solely due to plasma production.

Although great care was taken to getting a high sensitivity, no convincing proof of subthreshold signals from the investigated samples were found. The measured thresholds of strongly and weakly absorbing media did very well coincide when comparing the two main techniques discussed in this report (SPT, TIR-based PAD/PTD). Therefore, the existence of subthreshold precursor signals that do correlate with upcoming damage cannot be confirmed (in disagreement with several experiments detailed in literature)

A statistical analysis of scatter increase, visible plasma and acoustic wave amplitude emanating from the sample surface of BK7 showed a perfect correlation between those three phenomena. The information given is complementary and allows to analyze the underlying process.

The publication in a refereed journal is planned in 2001, where SPT and the newly developed TIR based PAD/PTD will be presented and applied to different types of media.

7. Literature

[Becker] M.F.Becker et al., „Charge emission and related precursor events associated with laser damage“, in Fifteenth Annual Symposium on optical materials for high-power lasers, NBS US Spec. Pub (1983).

[Clark] S.E.Clark et al., “The early detection of laser–induced damage”, J. Phys. E: Sci. Instrum. 22, 466 (1989).

[Domann_a] F.E.Domann, “Laser induced particle emission as a precursor to laser damage”, NIST Spec. Pub 756, 176 (1987).

[Domann_b] F.E.Domann, “Charged particle emission related to laser damage”, Appl. Opt. 25 1371 (1986)

[Domann_c] F.E.Domann, “Laser induced particle emission as a precursor to laser damage”, Appl. Opt. 27, 4423 (1988).

[Franck] J.B.Franck et al., “Automated pulsed testing using a scatter-probe damage monitor”, in Laser Induced Damage in Optical Materials: 1984, ed. By H.E.Bennett, A.H.Guenther, et al., Washington DC, NBS Special Publication 727, p. 71 ff.

[ISO] ISO/DIS 11 254-1.2 / 2 “Optics and optical instruments – laser and laser related equipment – Test methods for laser induced damage threshold of optical surfaces – Part 1: 1 on 1 test / Part 2: S on 1 test.

[Petzoldt] S. Petzoldt et al., “Surface laser damage thresholds determined by photoacoustic deflection”, Appl. Phys. Lett. 53, p. 2005 – 7 (1988).

[Porteus] Porteus et al., “Correlation between He-Ne scatter and 2.7 µm pulsed laser damage at coating defects”, Appl. Opt. 25, 3871 (1986).

[Riede] W. Riede et al., “Laser-induced damage measurements according to ISO/DIS 11254-1: results of a national Round Robin experiment on Nd:YAG laser-optics, SPIE Vol. 3244, pp. 96 – 103 (1998).

[Rosencwaig_a] A. Rosencwaig et al., “Photoacoustic absorption measurements of optical materials and thin films”, J. Appl. Phys. 51, 4361 (1980).

[Rosencwaig_b] A. Rosencwaig et al., ”Photoacoustic study of laser damage in thin films”, Appl. Phys. Lett. 36, 667 (1980).

[Rosencwaig_c] A. Rosencwaig et al., “Real-time laser damage monitoring with photo-acoustics”, Appl Opt. 19, 4133 (1980).

[Vouagner] D. Vouagner et al., “A new method to determine laser damage threshold for thin diamond-like carbon films on silicon”, Diamond and related materials 9, 786 (2000).

[Welsch] E. Welsch et al., “Application of photothermal probe beam deflection technique for the high-sensitive characterization of optical thin films with respect to their optical, thermal and thermoelastic inhomogeneities”, International Symposium on Optical Interference Coatings, Grenoble, France 1994.

[Willamowski] U. Willamowski et al., “Untersuchungen zur ISO-Standardmessverfahren zur Charakterisierung optischer Komponenten” EUREKA-Verbundprojekt CHOCLAB (1998).

8. Appendix

8.1 VEE software tool for data processing

During work for EOARD contract a software tool based on VEE Pro was developed that is used for applying statistical methods on measured data. Given a certain threshold amplitude, all fluence values will get the attribute damage (value 1) or no damage (value 0) when the signal amplitude is larger or smaller than that a preset threshold. The data set is then distributed into fluence intervals and for each of them the probability of damage has to be calculated. To analyze the threshold according to ISO 11254 1.2 / 2.0, a linear regression is implemented in this tool.

This software tool is considered to be very useful as it reduces the amount of influence of the "operator" of the experiment on the measured damage threshold. The only influence the operator has is the selection of the width of fluence intervals and the number of fluence intervals that are used for calculating the linear fit, which should be done for the first few data points above zero probability. The following Fig. 8.1 shows the panel view of this software tool.

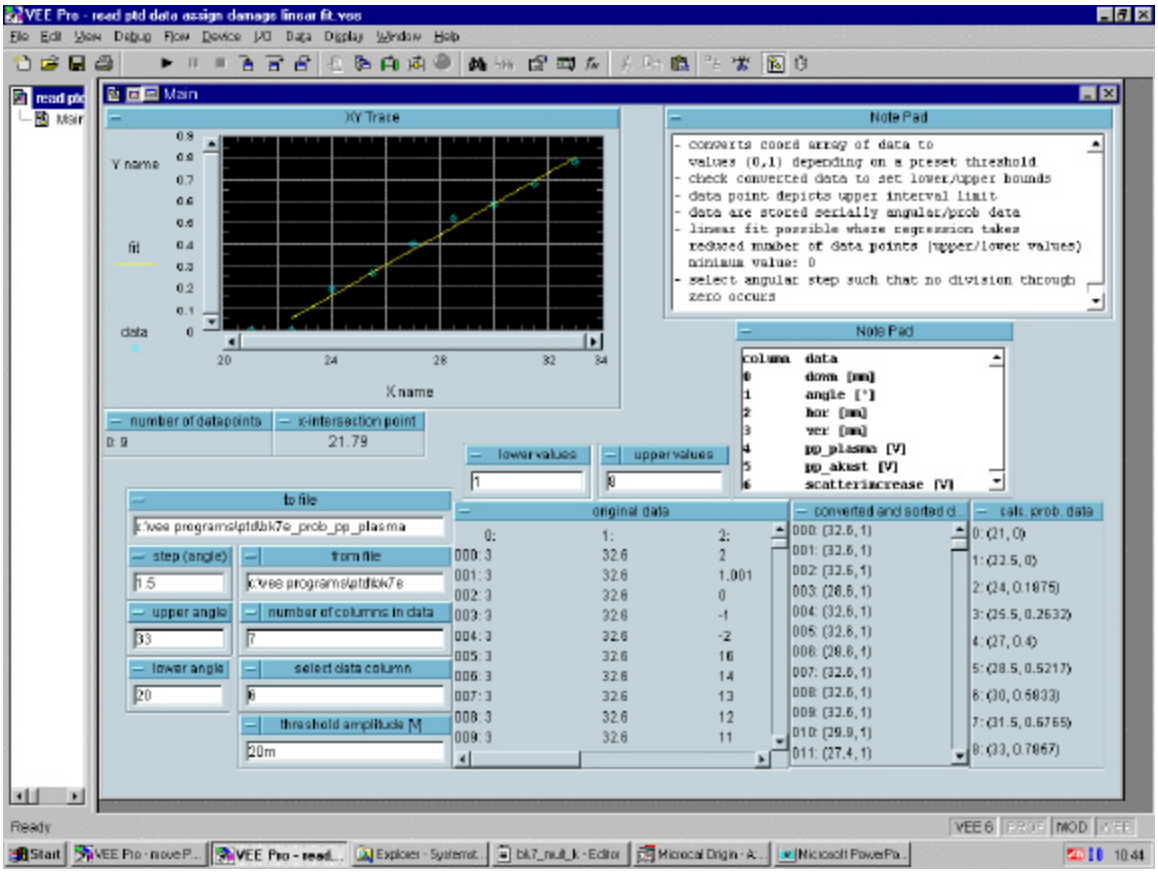

Fig. 8.1 VEE Pro software tool used to handle damage threshold relevant data using statistical methods.

8.2 Online damage monitor

According to measurements of acoustic signals of both front and back surface a simple damage monitoring set-up can be proposed (Fig. 8.2). The discrimination of front and back surface signals can simply be done by passing the probe laser beam at different distances a, b from the surface (Fig. 5.12).

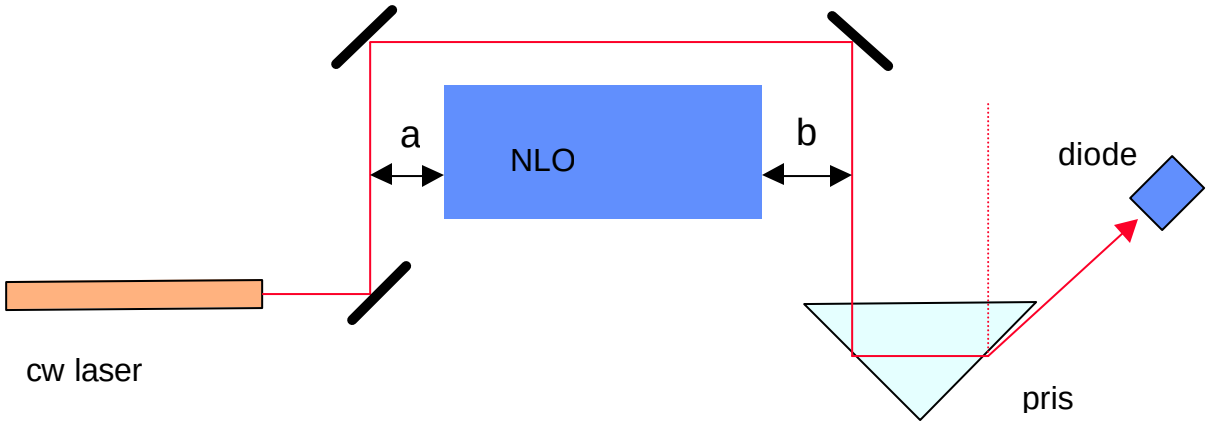

Fig. 8.2 Online damage monitor

Provided that the shock waves originating from the surfaces have approximately similar average velocities v_a, v_b , then the corresponding signals will be measured at times $t_a = a/v_a$ and
$t_b = b/v_b$ after a trigger signal (laser pulse) at t_0. At several mm distance from the surface, the velocity is identical to velocity of sound (Fig. 5.6). Acoustic signals should be used as they propagate faster (i.e. their response time is shorter), their onset threshold usually lower than thermal signals, and the thermal amplitude decays more rapidly during propagation as it is diffusion based.

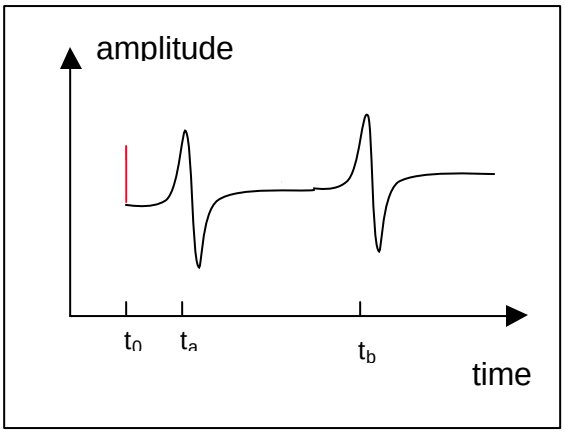

Fig. 8.3 Acoustic signal from different surfaces after a trigger signal at t_0.

The delay of the shock wave with reference to the laser pulse is a function of fluence, but the variation is on the order of a few µs (Fig. 8.4)

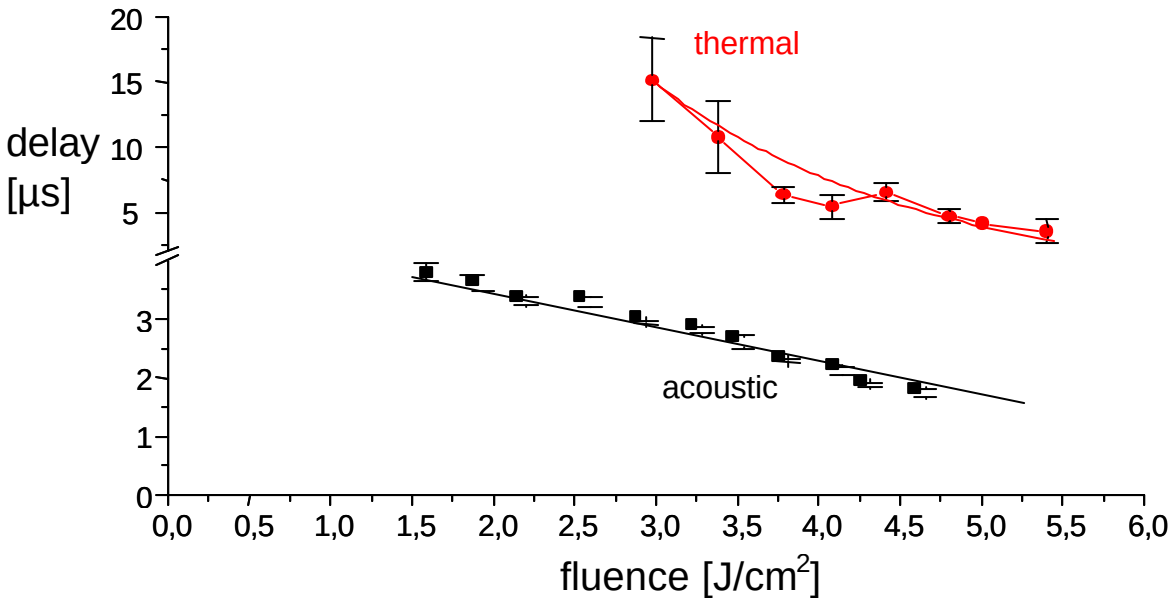

Fig. 8.4 Shock wave delay measured 1 mm above Si as a function of applied fluence.

The experiments confirmed that typically, damage propagates into the bulk of the sample, starting from some small damage spot on surface into the bulk of the sample under multipulse exposure. The following picture (Fig. 8.5) shows a $LiNbO_3$ crystal which has a damage channel all along its crystal axis. If irradiation would have stopped right after the onset of damage on the rear surface, the crystal would still be useful after repolishing. With severe bulk damage like this, the crystal is ruined.

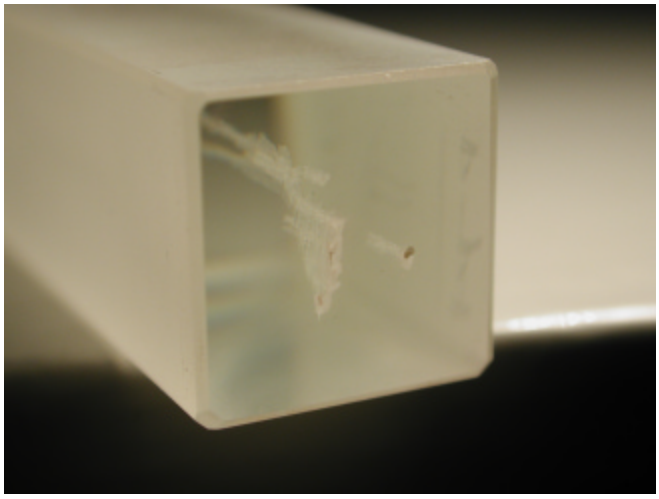

Fig. 8.5 Back face of $LiNbO_3$ OPO crystal with bulk damage penetrating into the crystal, starting from surface damage.

Surface evaluation of laser-irradiated coated / uncoated MIR optronic components

Wolfgang Riede
DLR Stuttgart
Institute of Technical Physics
Pfaffenwaldring 38 – 40
70 569 Stuttgart
Germany

6. Summary and outlook

In this report results of laser damage threshold measurements at typical MIR optical components (Ge, Si, ZnSe, sapphire) are summarized. These components were damage tested under out-of-band, pulsed irradiation at 1.06 µm.

A new technique of monitoring laser-induced shock waves and thermal waves above the sample surface called TIR-based PAD/PTD was developed and tested and found to be a sensitive and practical tool.

With PAD detection selective monitoring of several sample surfaces of optical components can be realized, irrespective of their thickness. Therefore, PAD might be used as a tool for online monitoring of expensive laser crystals or nonlinear-optical systems to prevent irreversible damage. A corresponding damage monitor has been proposed.

TIR-based PAD/PTD technique has been applied to materials having a very low LIDT due to very strong absorption and BK7, where the damage mechanism was identified being solely due to plasma production.

Although great care was taken to getting a high sensitivity, no convincing proof of subthreshold signals from the investigated samples were found. The measured thresholds of strongly and weakly absorbing media did very well coincide when comparing the two main techniques discussed in this report (SPT, TIR-based PAD/PTD). Therefore, the

existence of subthreshold precursor signals that do correlate with upcoming damage cannot be confirmed (in disagreement with several experiments detailed in literature)

A statistical analysis of scatter increase, visible plasma and acoustic wave amplitude emanating from the sample surface of BK7 showed a perfect correlation between those three phenomena. The information given is complementary and allows to analyze the underlying process.

The publication in a refereed journal is planned in 2001, where SPT and the newly developed TIR based PAD/PTD will be presented and applied to different types of media.